

# UNIFYING LONG AND SHORT SPATIO-TEMPORAL FORECASTING WITH SPECTRAL GRAPH NEURAL NETWORKS

**Anonymous authors**

Paper under double-blind review

## ABSTRACT

Multivariate Time Series (MTS) forecasting plays a vital role in various practical applications. Current research in this area is categorized into Spatial-Temporal Forecasting (STF) and Long-term Time Series Forecasting (LTSF). While these tasks share similarities, the methods and benchmarks used differ significantly. Spatio-Temporal Graph Neural Networks (STGNNs) excel at modeling interrelationships in STF tasks but face difficulties with long sequence inputs due to inefficient training. In contrast, LTSF models handle long sequences well but struggle with capturing complex variable interrelationships. This paper proposes the Spectral Spatio-Temporal Graph Neural Network (S2GNN) to address these challenges, unifying short- and long-sequence spatio-temporal forecasting within a single framework. *S2GNN leverages a decoupled GNN along with an MLP architecture to ensure efficiency. Specifically, it employs spectral GNNs for global feature extraction on an adaptive graph structure and uses MLP to process multiple feature embeddings, enabling it to handle varying sequence lengths.* Additionally, we introduce scale-adaptive node embeddings and cross-correlation embeddings for better differentiation between similar temporal patterns. Extensive experiments on eight public datasets, including both STF and LTSF datasets, demonstrate that S2GNN consistently outperforms state-of-the-art models across diverse prediction tasks. Code is available at <https://anonymous.4open.science/r/S2GNN-B21D>.

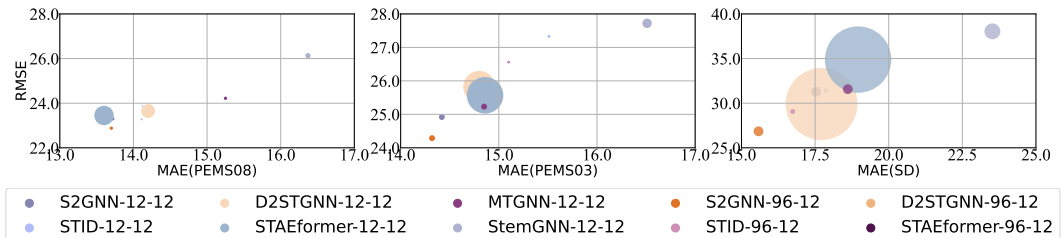
## 1 INTRODUCTION

Current Multivariate Time Series (MTS) prediction methods can be broadly categorized into Spatio-Temporal Forecasting (STF) and Long-term Time Series Forecasting (LTSF) (Shao et al., 2023). STF focuses on capturing both spatial and temporal dependencies, with Spatio-Temporal Graph Neural Networks (STGNNs) being a prominent approach (Jiang et al., 2023). These models are commonly evaluated on spatio-temporal datasets, such as those from the PEMS (Chen et al., 2001) traffic series. In contrast, LTSF emphasizes learning patterns like seasonality or trends over longer input sequences and utilizes long-sequence datasets that cover a wide range of scenarios to ensure robust model generalization (Qiu et al., 2024; Zhou et al., 2021).

The key distinction between these two research areas lies in their ability to process input sequences. STF models are typically designed for short-term inputs and may struggle with longer sequences, partly due to the high training costs associated with some models (Han et al., 2024). On the other hand, LTSF models are better suited for handling longer input sequences but often face challenges in capturing spatio-temporal relationships and tend to incur high computational complexity, especially when using transformer-based architectures (Huang et al., 2023). Figure 1 shows the performance of several STF models on short-term and long-term inputs. As the figure indicates, the FLOPs of most models increase significantly with input length, making long-term training nearly impossible. Thus, there is a clear need for an STGNN model capable of handling both short and long input sequences efficiently.

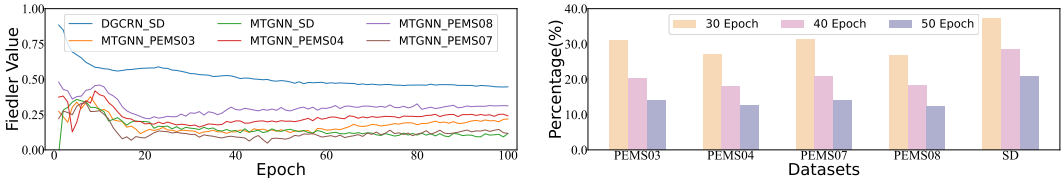
As a crucial part of STGNN models, most existing approaches rely on GCN-based methods (Kipf & Welling, 2016). However, current research in GNNs mainly follows two directions: spatial-based

054 and spectral-based approaches (Guo & Wei, 2023). Spatial GNNs capture node representations  
 055 through message passing and aggregation among neighboring nodes, often acting as low-pass fil-  
 056 ters (Wu et al., 2019a). In contrast, spectral-based GNNs perform convolutions in the spectral  
 057 domain of the graph Laplacian, offering more flexibility in handling different frequency compo-  
 058 nents (He et al., 2021). In dynamic or evolving graphs, spectral GNNs may be less robust due  
 059 to their reliance on the graph Laplacian, which is sensitive to changes in the graph structure. As  
 060 a result, spatial GNNs are often employed in existing work to learn spatial relationships between  
 061 variables (Zheng et al., 2024), though we explore whether this assumption holds universally in this  
 062 paper.



072 **Figure 1: Comparison of existing models on short-term STF and long-term STF results. From left to right, the number of nodes increases across three datasets. The size of the circles represents the FLOPs required to train for one epoch. Existing models struggle to balance prediction accuracy and training efficiency when handling long-term STF tasks.**

077 To address the limitation of static graph structures in capturing dynamic changes in nodes, as well  
 078 as the use of spatiotemporal models in scenarios without graph structures, adaptive graph structures  
 079 are widely used in STGNNs and are typically assumed to change continuously throughout training,  
 080 making spectral GNNs seem impractical for dynamic environments due to their sensitivity to graph  
 081 structure changes. This raises an interesting question: how much do adaptive graph structures, often  
 082 constructed using randomly initialized node embedding vectors, actually change during training?  
 083 Figure 2 illustrates the training process of two existing models that use adaptive graph structures.  
 084 Evidence across various datasets shows that, contrary to common belief, both the connectivity and  
 085 numerical variations of the adaptive graphs stabilize gradually in training. This observation chal-  
 086 lenges the assumption that spectral GNNs are too sensitive and motivates the use of spectral GNNs  
 087 with learnable filters on adaptive graph structures. Additionally, from the perspective of perturba-  
 088 tion theory for eigenvectors, if the change in the corresponding eigenvalue is sufficiently small, the  
 089 eigenvector will not shift significantly (Spielman, 2019).



096 **Figure 2: Observations of adaptive graph structure in STF datasets. Left: The changes in the connectivity of the graph structure tend to stabilize as the number of epochs increases. Right: The difference in the percentage of Frobenius norm between the best epoch and the 30th, 40th, and 50th epochs, respectively.**

101 Meanwhile, for the sake of training efficiency, we adopt a simple yet effective model architecture for  
 102 the sequential modelling. We review the concept of sample indistinguishability, which first proposed  
 103 in (Deng et al., 2021). Although previous work has addressed the indistinguishability in the temporal  
 104 and spatial domains separately (Shao et al., 2022a), we believe that the current approaches still have  
 105 certain limitations. Firstly, existing methods for handling spatial distinguishability cannot adapt to  
 106 changes in the number of nodes. Learning node representations in a fixed  $d$ -dimensional feature  
 107 space becomes more challenging as the number of nodes increases. Secondly, embedding methods  
 using temporal information are influenced by the sequence’s periodicity, and incomplete temporal

data can reduce the model’s ability to distinguish patterns. Thus, an embedding method that directly learns distinguishable features from the input sequence is needed.

To address the first issue, we use sparse initialization for node embeddings, leveraging the Restricted Isometry Property (RIP) theory (Tropp, 2017) to link sparsity with the number of nodes, allowing the embeddings to adapt to changes in node scale. For the second issue, we compute cross-correlation between the input and feature sequences to learn features adaptively. This dynamic addition of feature embedding vectors enhances the model’s ability to resolve sample indistinguishability.

**Our contributions.** In summary, our main contributions are as follows:

- We propose the Spectral Spatio-Temporal Graph Neural Network (S2GNN), which incorporates learnable filters capable of adaptively capturing and processing both short- and long-sequence features, enhancing the model’s expressiveness and versatility. [The decoupled GNN along with an MLP architecture ensures overall efficiency.](#)
- We introduce a scale-adaptive node embedding method that leverages sparsity to accommodate varying node scales and a cross-correlation embedding method that adaptively learns to distinguish features from the input sequences.
- Experimental results reveal that both low-pass and high-pass information must be considered when using learnable filters in conjunction with the adaptive graph. Meanwhile, our model balances training efficiency and performance, achieving superior results on eight public datasets compared to existing models.

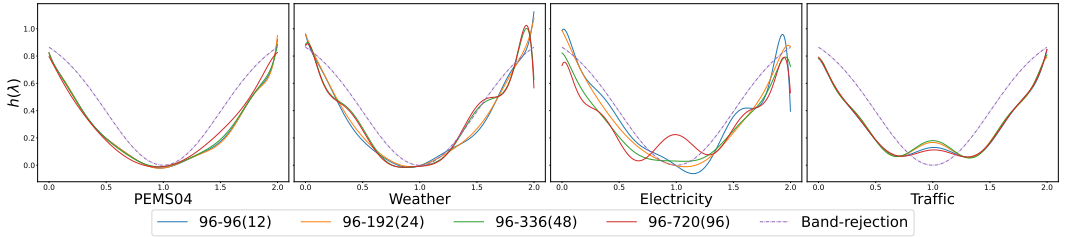


Figure 3: Visualization of learned graph filters. The results show that the filters of the adaptive graph resemble a band-rejection filter across all public datasets, indicating the presence of both homophilic and heterophilic relationships between nodes.

## 2 PRELIMINARIES

### 2.1 SPECTRAL GRAPH NEURAL NETWORK

Spectral GNNs work in the frequency (spectral) domain using graph Laplacian, which enables them to apply various filters to the graph signal (node features) (Bruna et al., 2013). The graph filters could be fixed (Kipf & Welling, 2016) (Klicpera et al., 2018) (Wu et al., 2019a) or approximated with polynomials (Defferrard et al., 2016) (Chien et al., 2020) (He et al., 2021). Spectral graph models naturally excel at learning heterophilic relationships. Since the homophilic/heterophilic relationships in adaptive graphs are uncertain, spectral models are well-suited for use on adaptive graphs if we can ignore their dynamic changes. Among existing spectral GNNs, **ChebNetII** (He et al., 2022) can approximate an arbitrary spectral filter  $h(\lambda)$  with an optimal convergence rate, and the learnable parameter  $\gamma_j$  allows the model to learn an arbitrary spectral filter via gradient descent. Additionally, it offers strong interpretability. It is formulated as:

$$\mathbf{Y} = \frac{2}{K+1} \sum_{k=0}^K \sum_{j=0}^K \gamma_j T_k(x_j) T_k(\hat{\mathbf{L}}) f_\theta(\mathbf{X}) \tag{1}$$

where  $x_j = \cos((j+1/2)\pi/(K+1))$  and the Chebyshev nodes of  $T_{K+1}$ ,  $f_\theta(\mathbf{X})$  denotes an MLP on the node feature matrix  $\mathbf{X}$ , and  $\gamma_j$  for  $j = 0, 1 \dots, K$  are the learnable parameters.

## 2.2 MULTIVARIATE TIME SERIES FORECASTING

Multivariate time series forecasting covers a wide range of methods. Solely from the perspective of explicitly leveraging inter-variable relationships, models can be broadly categorized into GNN-based models, cross-variable interaction models and cross-time interaction models. First, we provide some definitions to facilitate a quicker understanding of the relevant concepts.

**Time series.** A time series  $\mathbf{X} \in \mathbb{R}^{N \times T}$  is a time oriented sequence of  $N$ -dimensional time points, where  $T$  is the number of time points, and  $N$  is the number of variables. When  $N = 1$ , a time series is called univariate. When  $N > 1$ , it is called multivariate.

**Spatial-Temporal Forecasting (STF)** primarily focuses on modeling the temporal and spatial patterns of multivariate time series. Let  $G = (\mathcal{V}, \mathcal{E})$  be a network as an undirected graph with  $V = |\mathcal{V}|$  nodes and  $E = |\mathcal{E}|$  edges. It involves learning a model  $f$  that, given observations of historical look-back observations  $\mathbf{X} \in \mathbb{R}^{V \times P}$  of  $P$  timesteps on a graph  $G$ , outputs predictions  $\mathbf{Y} \in \mathbb{R}^{V \times F}$  for the future horizon of length  $F$ . The process is defined as:

$$[x_{t-P+1}, \dots, x_{t-1}, x_t; G] \xrightarrow{f_\theta} [x_{t+1}, x_{t+2}, \dots, x_{t+F}]$$

where  $x_t \in \mathbb{R}^V$  is a graph signal vector at time step  $t$ ,  $\theta$  is a collection of learnable parameters. In this paper, the number of nodes is equal to the number of variables, i.e.,  $N = V$ .

**Long-term Time Series Forecasting (LTSF)** primarily focus on modeling the long-term dependencies of multivariate time series. The definition of LTSF is similar to STF, except that it does not explicitly use a graph structure and typically involves a longer input data sequence.

With the development of GCN (Defferrard et al., 2016) (Kipf & Welling, 2016), models begin to utilize GCNs to model spatial dependencies based on a pre-defined prior graph and further combine them with sequential models (Yu et al., 2017) (Li et al., 2017) (Wu et al., 2019b). However, many recent works argue that the pre-defined prior graph might be biased, incorrect, or even unavailable in many cases. Thus, they propose to jointly learn the graph structure (i.e., adaptive graph) (Bai et al., 2020) (Jin et al., 2022) (Shang et al., 2021) or use graph-free methods to do STF tasks (Shao et al., 2022a) (Liu et al., 2023b) (Deng et al., 2021).

Cross-variable interaction models are also critical for time series forecasting. Recently, (Zhang & Yan, 2023) and (Liu et al., 2023c) both adopted channel-wise Transformer-based frameworks, and extensive experimental results have demonstrated the effectiveness of channel-wise attention for time series forecasting.

Cross-time interaction models focus on extracting information along the time dimension, such as patch-wise patterns (Nie et al., 2022), multi-scale information (Wang et al., 2024) (Shabani et al., 2022), or frequency-domain features (Wu et al., 2021) (Piao et al., 2024).

## 3 METHODOLOGY

In this section, we first briefly review the concept of sample indistinguishability, and then we present our proposed embedding methods. Next, we introduce the adaptive graph structure widely used in the field of STF, as well as how graph filters are applied to this structure. Finally, we provide an overall illustration of the S2GNN architecture and the prediction module, which consists of multiple MLPs.

### 3.1 INDISTINGUISHABILITY OF TIMES SERIES SAMPLES

Simply speaking, sample indistinguishability occurs when dynamics from different factors overlap, making input sequence features too similar to distinguish. (Deng et al., 2021) points out that this issue hinders deep neural networks from capturing spatial and temporal differences, while (Shao et al., 2022a) offers a simple framework to mitigate it. In this paper, we introduce a scale-adaptive node embedding method to adapt the model to varying node numbers and a cross-correlation embedding method to extract distinguishable features directly from the input sequence, addressing cases where temporal information is unavailable or ineffective.

**Scale-Adaptive Node Embeddings.** (Yeh et al., 2024) shows that random projection can enhance a model’s ability to capture spatial relationships within input sequences. In our work, we leverage this

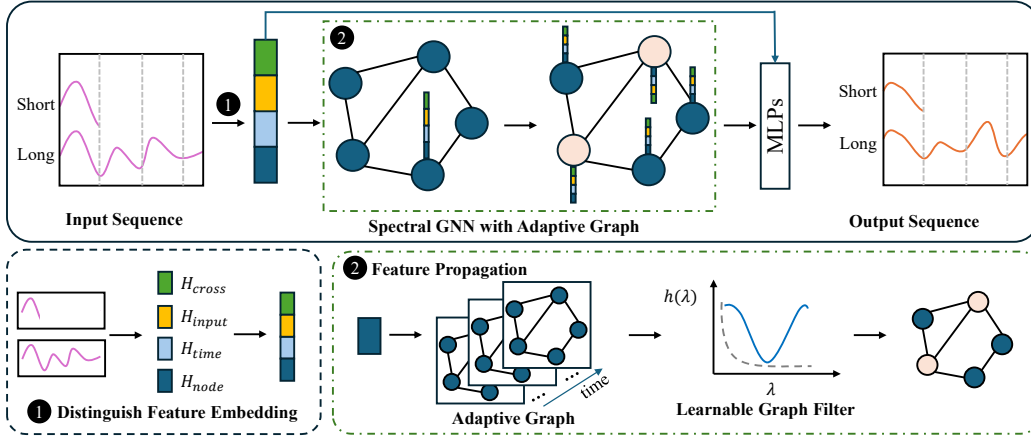


Figure 4: Overall architecture. We first extract distinguishable features from the input sequence and then propagate these features on an adaptive graph while learning filters suited to the adaptive graph. Finally, we use multi-layer MLPs for learning. The overall structure of S2GNN is simple yet effective, allowing it to handle both short-term and long-term STF tasks.

approach along with sparse initialization to generate node embeddings. The benefit of this method is that under the Restricted Isometry Property (RIP) (Tropp, 2017) theory, we can use sparsity to link the number of nodes with the node embeddings. It allows the dimensionality of the node embeddings used in training to remain within a smaller range ( $h \ll N$ ), bypassing the increased learning difficulty caused by a larger number of nodes. Assuming  $r \in (0, 1)$  represents sparsity, the dimension  $h$  of the random projected matrix should satisfy:

$$h = c \cdot r \log(N/r). \quad (2)$$

Where  $c$  is a constant,  $N$  represents the number of nodes. Therefore, our Scale-Adaptive Node Embeddings is formulated as following:

$$\begin{aligned} \hat{\mathbf{W}}_{\text{node}} &= \text{Linear}_1(\text{Linear}_2(\mathbf{W}_{\text{node}}^T))^T, \\ \mathbf{H}_{\text{node}} &= \hat{\mathbf{W}}_{\text{node}}[\mathbf{X}_{\text{node}}], \end{aligned} \quad (3)$$

where  $W_{\text{node}}$  and  $\hat{W}_{\text{node}} \in \mathbb{R}^{N \times d}$  and  $\text{Linear}_2$  refers to fixed random projection operation. It is noticed that our randomly initialized node embeddings  $W_{\text{node}}$  are fixed and do not participate in training process, which is different from existing methods.  $X_{\text{node}}$  represents node ID in the input sequence.

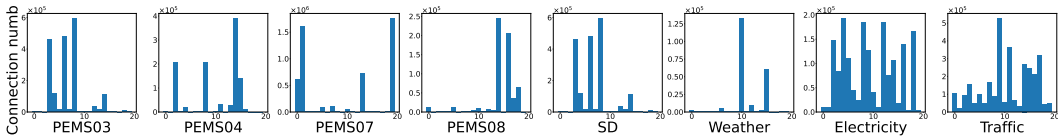


Figure 5: The connection number of each kernel in each dataset. The distribution demonstrates that the cross-correlation embedding method effectively distinguishes the input sequences.

**Cross-Correlation Embeddings.** The key to alleviating sample indistinguishability is to map a certain feature of the input sequence to an embedding vector using a meaningful value. This value could be the node’s ID, the time of the day, or the day of the week. To avoid relying on external information, we calculate the cross-correlation between the input sequence and a set of feature sequences. The input sequence is then connected to embedding vectors based on the magnitude of the cross-correlation. The calculation process can be efficiently achieved using convolution operation, as it inherently performs cross-correlation operation.

$$\begin{aligned} \mathbf{C}_t &= \text{Cross-Correlation}(\mathbf{X}_{t-L+1:t}, k_i), \\ \mathbf{H}_{\text{cross}} &= \mathbf{W}_{\text{cross}}[\text{argmax}(\mathbf{C}_t)], \end{aligned} \quad (4)$$

where  $k_i$  refer to the kernel in convolution. The index corresponding to the maximum value from multiple convolution operations is then selected as the index for the corresponding feature embedding matrix.

A more complex convolutional neural network could be designed to learn distinguishable features from the input sequence as long as it produces a value for indexing. However, for simplicity, we use a convolution kernel with the same length as the input sequence so that we can directly validate the cross-correlation embedding method and visualize the kernel to see the distinguishing features. Figure 5 shows the number of times each feature sequence is selected in the test set. Multiple feature sequences are chosen across different datasets, confirming the effectiveness of our method. Figure 6 shows the learned distinguishable features, where the color intensity of each sequence corresponds to the number of connections. The diversity of these features is clearly visible.

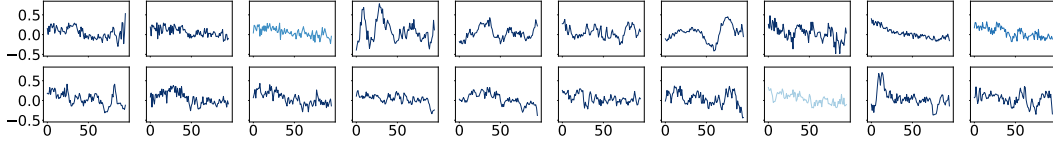


Figure 6: A visualization of the convolutional kernels used in the cross-correlation embedding process, where the color intensity represents their usage frequency (i.e., the number of times each kernel is connected).

### 3.2 ADAPTIVE ADJACENT MATRIX IN TIME SERIES

The term "adaptive graph structure" generally refers to any adjacency matrix derived from the node embeddings. In existing works, it is common to initialize a set of node embeddings as source nodes and another set of node embeddings as target nodes, followed by employing various computation methods to obtain an adjacency matrix that can be adapted during training. In this paper, we adopt the most straightforward approach: we directly represent each node's embedding with a set of trainable weights and compute the cosine similarity between node embeddings as the dynamic adjacency matrix. The calculation of the adjacent matrix and its Laplacian matrix are as follows:

$$\begin{aligned} \mathbf{A} &= \text{ReLU}(\text{CosineSimilarity}(\hat{\mathbf{W}}_{\text{node}})) \\ \mathbf{L} &= \mathbf{I} - \mathbf{D}^{-1/2} \mathbf{A} \mathbf{D}^{-1/2} \\ \hat{\mathbf{L}} &= 2\mathbf{L} / \lambda_{max} - \mathbf{I}, \end{aligned} \quad (5)$$

where  $\lambda_{max}$  is the largest eigenvalue of  $\mathbf{L}$ . Suppose we have the distinguishable features  $\mathbf{H}$ , then the propagation process on the adaptive graph is formulated as:

$$\mathbf{Z} = \frac{2}{K+1} \sum_{k=0}^K \sum_{j=0}^K \gamma_j T_k(x_j) T_k(\hat{\mathbf{L}}) \mathbf{H}, \quad (6)$$

where  $\gamma_j$  for  $j = 0, 1, \dots, K$  are the learnable parameters.  $x_j = \cos((j+1/2)\pi/(K+1))$  and the Chebyshev nodes of  $T_{K+1}$ , we set  $K = 10$  as a default hyperparameter.

### 3.3 OVERALL STRUCTURE

In total, we have multiple feature embeddings concatenated altogether as distinguishing feature embeddings. Moreover, we concatenate the propagated feature embeddings with the original ones. This approach is as follows:

$$\begin{aligned}
\mathbf{H} &= \mathbf{H}_{\text{input}} \parallel \mathbf{H}_{\text{node}} \parallel \mathbf{H}_{\text{time}} \parallel \mathbf{H}_{\text{cross}} \\
\mathbf{Z} &= \text{SpectralGNN}(\mathbf{H}) \\
\hat{\mathbf{Z}} &= \text{Concat}(\mathbf{H}, \text{Linear}(\mathbf{Z})).
\end{aligned}
\tag{7}$$

We use  $\hat{\mathbf{Z}}$  obtained from above as the input for the prediction module. The overall structure of the prediction module is a stack of MLPs, each with a residual connection. In the end, we obtained the prediction results of another linear regression on the last layer. We use the mean absolute error (MAE) as the loss function on spatialtemporal datasets and the mean squared error (MSE) on long-sequence datasets:

$$\begin{aligned}
\hat{\mathbf{Z}}^{l+1} &= f_{\theta}(\hat{\mathbf{Z}}^l) + \hat{\mathbf{Z}}^l \\
\hat{\mathbf{Y}} &= \text{Linear}(\hat{\mathbf{Z}}^{\text{last}}).
\end{aligned}
\tag{8}$$

## 4 EXPERIMENTS

In this section, our primary goal is to demonstrate the effectiveness and feasibility of S2GNN in handling both long and short sequence inputs. We first introduce the basic experimental setup, followed by presenting the results of S2GNN on real-world data. Afterward, we compare the computational cost of training S2GNN and baseline models for one epoch across various datasets. Although different models require varying total epochs for training and have different memory demands, the comparison of FLOPs still provides an intuitive reflection of the challenges faced during model training. Finally, we visualized the prediction results of S2GNN and the baseline models on certain datasets. From these visualizations, we were able to identify some of the reasons why existing models fail in specific scenarios.

### 4.1 EXPERIMENT SETTINGS

**Datasets.** We conducted experiments on eight real-world datasets, including five traffic flow datasets commonly used in spatio-temporal forecasting tasks (PEMS03, PEMS04, PEMS07, PEMS08, and SD) and three benchmark datasets typically employed for long-term time series forecasting tasks (Electricity, Weather, and Traffic).

**Baselines.** We selected several existing spatiotemporal models and compared their performance on both short-term and long-term inputs in Figure 1. Among these, D2STGNN (Shao et al., 2022b) require pre-defined graph structures, while StemGNN (Cao et al., 2020) and MTGNN (Wu et al., 2020) employs an adaptive graph structure. Although STID (Shao et al., 2022a) and STAEformer (Liu et al., 2023a) do not utilize graph structures, they have demonstrated effectiveness in short-term STF tasks. Detailed results are in the appendix (Table 3).

For the LTSF tasks, we selected various types of models from the perspective of explicitly leveraging inter-variable relationships as benchmark baselines. DLinear (Zeng et al., 2022) is one of the simplest and most effective recent models. PatchTST (Nie et al., 2022) processes time series data by segmenting it into patches, which is widely adopted nowadays. MTGNN (Wu et al., 2020) has proven effective for both STF and LTSF. TimesNet (Wu et al., 2022) and iTransformer (Liu et al., 2023c) focus on leveraging relationships between variables for forecasting. CrossGNN (Huang et al., 2023) is a recently proposed spatial GNN model with linear complexity that balances both efficiency and predictive performance in LTSF tasks.

**Evaluation metrics.** Following previous work, for STF tasks, we compared the MAE, RMSE, and MAPE using the re-normalized prediction results, benchmarking against other models. For LTSF tasks, we used the normalized prediction results and compared the models based on MAE and MSE. To simplify the presentation of results across both STF and LTSF datasets, we omitted MAPE from the main text since the other two metrics used are sufficient to support the conclusions of the paper.

**Implementation details.** Our experiments were conducted on a 16GB V100 and a 40GB NVIDIA A100 GPU, averaging results over three random seeds. Due to the training efficiency of existing models and our computational resource limits, we reproduced only a subset of them. Our reproduced results on long-sequence data were slightly worse than those in the CrossGNN paper, so we

used their reported results for comparison. Most of our computational resources focused on the spatiotemporal datasets. For the spatiotemporal forecasting (STF) task, we used two settings: one with an input length of  $P = 12$  to predict the next  $F = 12$  steps and another with  $P = 96$  to predict future outputs at  $F = \{12, 24, 48, 96\}$  steps. For LTSF, we used  $P = 96$  to predict future results at  $F = \{96, 192, 336, 720\}$ . We used AdamW as the optimizer with a learning rate of 0.005 and trained each model for 100 epochs on each dataset, with a batch size of 64.

Table 1: Experimental results on long-term STF datasets and LTSF datasets.

Methods	Ours			iTransformer		CrossGNN		TimesNet		PatchTST		DLinear		MTGNN	
Metric	MAE	RMSE	MAE	RMSE	MAE	RMSE	MAE	RMSE	MAE	RMSE	MAE	RMSE	MAE	RMSE	
PEMS03	12	<b>14.32</b>	<b>24.29</b>	15.60	26.70	17.46	27.56	17.26	27.68	17.11	27.20	20.83	33.99	<u>14.64</u>	<b>23.91</b>
	24	<b>16.08</b>	<b>27.49</b>	<u>18.03</u>	<u>30.47</u>	22.34	35.41	19.66	31.65	21.21	34.09	29.50	49.12	66.62	101.44
	48	<b>18.90</b>	<b>32.95</b>	<u>22.36</u>	<u>37.80</u>	30.55	47.48	24.24	40.40	28.12	45.63	46.00	74.96	61.21	95.70
	96	<b>21.24</b>	<b>36.96</b>	<u>26.41</u>	<u>44.12</u>	41.98	62.41	30.18	50.73	36.50	58.39	69.01	103.58	82.78	114.90
PEMS04	12	<b>18.16</b>	<b>29.74</b>	20.31	32.43	23.84	37.31	21.48	33.80	26.08	40.80	27.06	42.75	<u>18.79</u>	<u>30.55</u>
	24	<b>19.21</b>	<b>31.28</b>	<u>22.63</u>	<u>35.84</u>	30.26	46.93	23.57	36.52	33.47	52.27	37.10	58.58	73.56	113.67
	48	<b>20.68</b>	<b>33.47</b>	<u>26.03</u>	<u>40.93</u>	42.15	63.62	26.93	41.65	47.73	73.46	56.16	87.05	52.26	89.81
	96	<b>21.47</b>	<b>34.63</b>	<u>30.35</u>	<u>47.58</u>	55.69	80.88	31.54	48.45	63.75	96.75	82.47	120.03	90.49	128.65
PEMS07	12	<b>19.10</b>	<b>32.21</b>	21.55	35.38	25.97	40.64	25.15	41.57	28.49	44.20	30.97	48.50	20.81	<u>33.83</u>
	24	<b>20.76</b>	<b>34.87</b>	24.71	40.50	33.76	51.55	28.30	40.09	37.03	57.61	44.42	69.55	<u>22.41</u>	<u>36.90</u>
	48	<b>22.96</b>	<b>38.36</b>	<u>29.05</u>	<u>47.53</u>	46.59	68.79	32.19	53.10	52.19	81.34	69.99	105.61	62.66	105.80
	96	<b>23.70</b>	<b>40.50</b>	<u>34.19</u>	<u>54.78</u>	60.42	85.12	37.41	62.42	65.03	102.00	105.04	143.06	109.37	151.35
PEMS08	12	<b>13.70</b>	<b>22.88</b>	15.15	24.73	18.62	29.52	19.08	30.82	20.60	32.29	21.60	34.37	<u>14.93</u>	<u>23.89</u>
	24	<b>14.87</b>	<b>24.88</b>	<u>17.00</u>	<u>27.96</u>	23.94	37.43	21.87	34.66	26.87	42.14	30.39	48.35	67.91	104.51
	48	<b>16.17</b>	<b>26.87</b>	<u>19.99</u>	<u>32.94</u>	32.55	49.32	27.13	42.44	37.75	58.65	48.37	74.35	47.88	82.05
	96	<b>17.36</b>	<b>28.88</b>	<u>23.35</u>	<u>38.27</u>	44.14	64.15	30.01	47.99	50.58	79.10	75.35	106.21	84.43	118.62
SD	12	<b>15.58</b>	<b>26.85</b>	17.30	<u>29.07</u>	23.44	39.19	19.64	32.50	23.09	37.82	28.26	49.85	<u>17.11</u>	29.50
	24	<b>17.96</b>	<b>32.19</b>	19.80	<u>33.98</u>	29.65	50.82	23.07	38.17	26.18	44.32	33.45	59.85	<u>19.77</u>	34.74
	48	<b>20.32</b>	<b>37.78</b>	<u>22.40</u>	<u>38.65</u>	34.22	58.41	23.35	39.33	27.06	45.69	36.61	65.24	59.00	101.37
	96	<b>21.82</b>	<b>40.65</b>	<u>24.68</u>	<u>43.81</u>	37.60	65.39	24.84	<u>42.19</u>	30.21	50.40	38.37	67.92	104.00	144.55
Metric	MAE	MSE	MAE	MSE	MAE	MSE	MAE	MSE	MAE	MSE	MAE	MSE	MAE	MSE	
Weather	96	<b>0.198</b>	<b>0.154</b>	0.211	0.175	0.218	0.159	0.220	0.172	0.230	0.171	0.255	0.196	0.329	0.230
	192	<b>0.243</b>	<b>0.200</b>	<u>0.253</u>	<u>0.210</u>	0.266	0.211	0.261	0.219	0.271	0.219	0.296	0.237	0.322	0.263
	336	0.304	0.277	<u>0.295</u>	<u>0.268</u>	0.310	<b>0.267</b>	0.306	0.280	0.321	<b>0.277</b>	0.335	0.283	0.396	0.354
	720	0.363	0.366	<b>0.351</b>	<b>0.343</b>	0.362	0.352	<u>0.359</u>	0.365	0.367	0.365	0.381	<u>0.345</u>	0.371	0.409
Electricity	96	<b>0.226</b>	<b>0.135</b>	<u>0.237</u>	<u>0.147</u>	0.275	0.173	0.272	0.168	0.268	0.159	0.276	0.194	0.318	0.217
	192	<b>0.244</b>	<b>0.154</b>	<u>0.255</u>	<u>0.166</u>	0.288	0.195	0.289	0.184	0.278	0.177	0.280	0.193	0.352	0.238
	336	<b>0.264</b>	<b>0.172</b>	<u>0.277</u>	<u>0.187</u>	0.300	0.206	0.300	0.198	0.296	0.195	0.296	0.206	0.348	0.260
	720	<u>0.305</u>	<u>0.215</u>	<b>0.299</b>	<b>0.214</b>	0.335	0.231	0.320	0.220	0.317	0.215	0.329	0.242	0.369	0.290
Traffic	96	<b>0.251</b>	0.508	<u>0.260</u>	<b>0.404</b>	0.310	0.570	0.321	0.593	0.319	0.583	0.396	0.650	0.437	0.660
	192	<b>0.263</b>	0.538	0.269	<b>0.428</b>	0.321	0.577	0.336	0.617	0.331	0.591	0.370	0.598	0.438	0.649
	336	<b>0.272</b>	<u>0.567</u>	<u>0.293</u>	<b>0.433</b>	0.324	0.588	0.336	0.629	0.332	0.599	0.373	0.605	0.472	0.653
	720	<b>0.285</b>	<u>0.596</u>	<u>0.287</u>	<b>0.431</b>	0.337	0.597	0.350	0.640	0.341	0.601	0.394	0.645	0.437	0.639

## 4.2 EXPERIMENT RESULTS

In Table 3, we demonstrate S2GNN’s capability in handling both long and short-sequence inputs for spatiotemporal forecasting tasks. Our proposed model not only achieves state-of-the-art prediction performance but also balances training efficiency. Furthermore, in Table 1, following the existing comparison methods for spatiotemporal forecasting and long-sequence prediction tasks, we compare the results of S2GNN with current models used for long-sequence prediction on both spatiotemporal and long sequence datasets.

Moreover, Figure 3 illustrates the shape of the graph filter learned by S2GNN. It can be observed that across all datasets (more results are in Figure 9), the graph filter exhibits a band-rejection filter shape, which strongly indicates that the adaptive graph contains both homophily and heterophily. This observation highlights that current methods using spatial GNNs limit the expressive capacity of the temporal adaptive graph. More specifically, on spatiotemporal datasets, the learned graph filter retains both low-frequency and high-frequency components while suppressing mid-frequency components, suggesting a strong polarization between homogeneity and heterogeneity. Therefore, we suspect that in typical spatiotemporal forecasting tasks, such as traffic flow prediction, ignoring odd-hop neighbors could theoretically enhance the robustness of spatial-GNN models (Lei et al., 2022). On multivariate datasets, however, the presence of mid-frequency components indicates that the polarization in the adaptive graph structure is less pronounced.

4.3 ABLATION STUDY

We performed ablation experiments on several datasets to assess the impact of distinguishable features, It can be seen that improving a model’s capacity to manage sample indistinguishability can boost its performance on STF. However, the scenario is more intricate with LTSF, possibly due to variations in data properties or evaluation standards.. Additionally, we stopped the gradient updates for the adaptive graph after training for 50 epochs. The results indicate that freezing the adaptive graph had a limited impact on prediction accuracy, suggesting that after a certain number of epochs, further structural changes in the adaptive graph no longer significantly influence the results. This consequence also supports the motivation behind our research.

Table 2: Ablation study. T: Temporal embedding. S: Scale-Adaptive node embedding. C: Cross-Correlaiton embedding. Stop-50: Stop the gradients of the adaptive graph after 50 epochs.

Methods	PEMS07		PEMS08		PEMS03		Electricity		Traffic	
	MAE	RMSE	MAE	RMSE	MAE	MSE	MAE	MSE	MAE	MSE
w/o T	27.20	44.31	19.37	30.93	21.80	34.75	0.236	0.144	0.267	0.535
w/o S	24.61	42.11	17.64	29.43	21.26	38.05	0.373	0.139	0.252	0.506
w/o C	25.12	41.83	17.55	29.07	21.66	37.64	0.224	0.133	0.250	0.510
stop-50	25.46	42.18	17.55	29.03	21.94	37.96	0.224	0.134	0.251	0.509
Ours	23.70	40.50	17.36	28.88	21.24	36.96	0.226	0.135	0.251	0.508

4.4 EFFICIENCY STUDY

We compared the number of parameters of existing models with the FLOPs required to train for one epoch. As shown in Figure 1, we selected tasks with different datasets (varying in node scale) and different prediction lengths for comparison. In the figure, the closer a model’s point is to the origin, the more worthwhile its computational efficiency. The size of each point reflects the MAE between the predicted results and the true values, where smaller points indicate better performance. It can be observed that S2GNN maintains stable performance across tasks with varying input and output lengths, effectively balancing prediction accuracy and training efficiency.

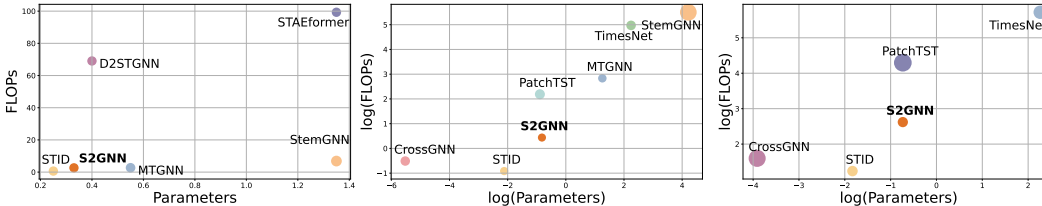


Figure 7: Comparison of FLOPs and total amount of parameters. From left to right are the results on the PEMS04 (12-12), PEMS08 (96-12), and PEMS07 (96-96) datasets. The size of the circles represents the MAE, smaller circles indicate better performance. FLOPs:  $\times 10^3$

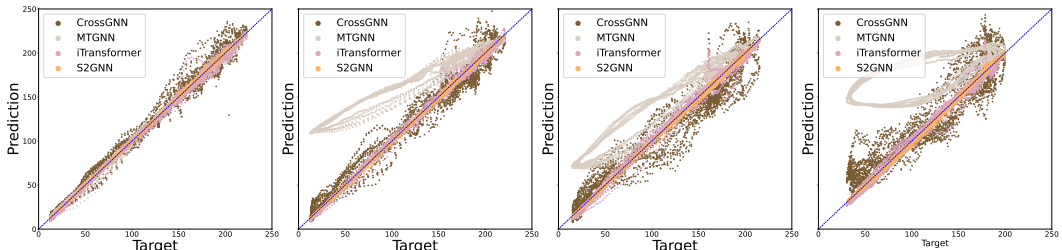
4.5 VISUALIZATION

In Figure 8, we show the results of S2GNN on both spatiotemporal and long-sequence datasets, along with a comparison to three existing models on the same tasks. Due to image size constraints, we selected one node’s results from each dataset for illustration. The horizontal axis represents the true values, while the vertical axis shows the predicted values. Ideally, all points should align along the diagonal line  $y = x$ , indicating perfect predictions.

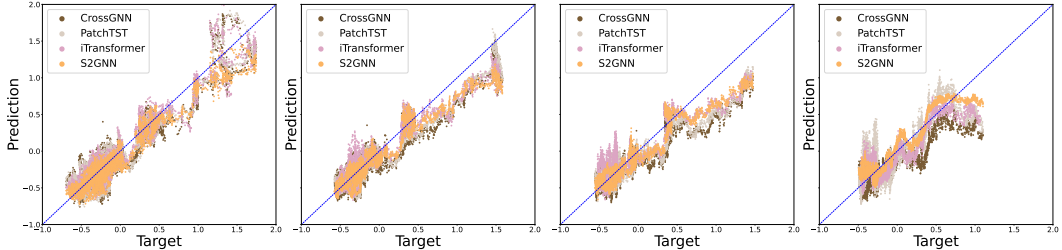
On spatiotemporal data, MTGNN cannot filter high-frequency information because it relies solely on spatial GNNs, resulting in predictions that are spread on both sides of the diagonal. This issue becomes increasingly evident as the output length increases. CrossGNN, on the other hand,

uses contrastive learning to handle homophilic and heterophilic information on the graph but still struggles with longer sequence forecasting. It tends to underpredict the true values, suggesting difficulty in handling distribution shifts over extended periods. Generally, S2GNN demonstrates a clear advantage in capturing both homophilic and heterophilic relationships in adaptive graphs due to learnable filters. It also maintains stable performance across long-sequence predictions compared with iTransformer, effectively balancing accuracy and adaptability.

On long-sequence data, S2GNN performs slightly worse than spatiotemporal data, possibly because the implicit graph structure in long-sequence data is less pronounced. Additionally, numerical effects introduced by normalization may also impact its performance. Despite this, S2GNN still shows smaller fluctuations compared to the other three models, with data points more tightly clustered around the diagonal. This stability becomes even more pronounced as the prediction length increases.



(a) Examples of PEMS04 dataset. We use the 200th node for the sake of simplicity. From left to right, the results depict predictions for 12, 24, 48, and 96 time steps based on an input sequence of 96.



(b) Examples of Electricity dataset. We use the 60th node for the sake of simplicity. From left to right, the results depict predictions for 96, 192, 336, and 720 time steps based on an input sequence of 96.

Figure 8: Comparison between the prediction results and the target values. Each data point represents the average of the predicted results and the true values over the given sequence.

## 5 CONCLUSION

In this paper, our research is motivated by the inefficiency of existing Spatio-Temporal Graph Neural Networks (STGNNs), which also struggle to handle long-sequence inputs. Through observing the training process of adaptive graphs in existing models, we found that their graph structures tend to stabilize after a few epochs. Based on this, we propose the Spectral Spatio-Temporal Graph Neural Network (S2GNN) to unify short-term and long-term STF while maintaining training efficiency. **The decoupled GNN along with an MLP architecture ensures overall efficiency.** Specifically, S2GNN incorporates learnable filters that adaptively capture both short-term and long-term features, improving the model’s expressiveness. To keep the model simple yet effective, we enhance its ability to handle indistinguishable samples by introducing a Scale-Adaptive node embedding method and a Cross-Correlation embedding method. These methods allow the node embeddings to adjust to varying numbers of nodes and learn distinguishable features directly from input sequences. Experiments on eight public datasets show that our model effectively addresses spatio-temporal prediction for both short and long sequences across different scenarios. It also suggests the importance of modeling both homophilic and heterophilic relationships in MTS forecasting.

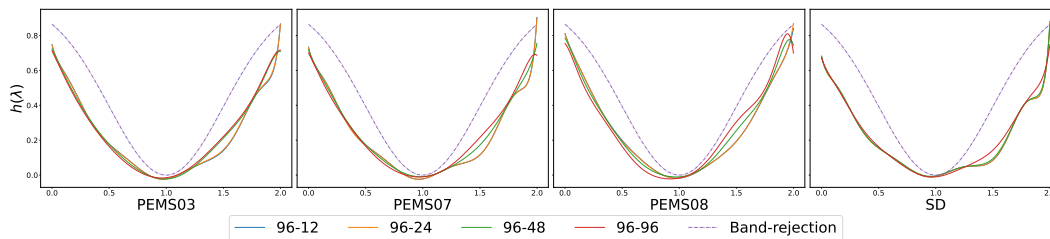
## REFERENCES

- 540  
541  
542 Lei Bai, Lina Yao, Can Li, Xianzhi Wang, and Can Wang. Adaptive graph convolutional recurrent  
543 network for traffic forecasting. *Advances in neural information processing systems*, 33:17804–  
544 17815, 2020.
- 545 Joan Bruna, Wojciech Zaremba, Arthur Szlam, and Yann LeCun. Spectral networks and locally  
546 connected networks on graphs. *arXiv preprint arXiv:1312.6203*, 2013.
- 547 Defu Cao, Yujing Wang, Juanyong Duan, Ce Zhang, Xia Zhu, Congrui Huang, Yunhai Tong, Bix-  
548 iong Xu, Jing Bai, Jie Tong, et al. Spectral temporal graph neural network for multivariate time-  
549 series forecasting. *Advances in neural information processing systems*, 33:17766–17778, 2020.
- 550 Chao Chen, Karl Petty, Alexander Skabardonis, Pravin Varaiya, and Zhanfeng Jia. Freeway perfor-  
551 mance measurement system: mining loop detector data. *Transportation Research Record*, 1748  
552 (1):96–102, 2001.
- 553 Eli Chien, Jianhao Peng, Pan Li, and Olgica Milenkovic. Adaptive universal generalized pagerank  
554 graph neural network. *arXiv preprint arXiv:2006.07988*, 2020.
- 555 Michaël Defferrard, Xavier Bresson, and Pierre Vandergheynst. Convolutional neural networks on  
556 graphs with fast localized spectral filtering. *Advances in neural information processing systems*,  
557 29, 2016.
- 558 Jinliang Deng, Xiusi Chen, Renhe Jiang, Xuan Song, and Ivor W Tsang. St-norm: Spatial and  
559 temporal normalization for multi-variate time series forecasting. In *Proceedings of the 27th ACM  
560 SIGKDD conference on knowledge discovery & data mining*, pp. 269–278, 2021.
- 561 Yuhe Guo and Zhewei Wei. Clenshaw graph neural networks. In *Proceedings of the 29th ACM  
562 SIGKDD Conference on Knowledge Discovery and Data Mining*, pp. 614–625, 2023.
- 563 Jindong Han, Weijia Zhang, Hao Liu, Tao Tao, Naiqiang Tan, and Hui Xiong. Bigst: Linear com-  
564 plexity spatio-temporal graph neural network for traffic forecasting on large-scale road networks.  
565 *Proceedings of the VLDB Endowment*, 17(5):1081–1090, 2024.
- 566 Mingguo He, Zhewei Wei, Hongteng Xu, et al. Bernnet: Learning arbitrary graph spectral filters via  
567 bernstein approximation. *Advances in Neural Information Processing Systems*, 34:14239–14251,  
568 2021.
- 569 Mingguo He, Zhewei Wei, and Ji-Rong Wen. Convolutional neural networks on graphs with cheby-  
570 shev approximation, revisited. *Advances in neural information processing systems*, 35:7264–  
571 7276, 2022.
- 572 Qihe Huang, Lei Shen, Ruixin Zhang, Shouhong Ding, Binwu Wang, Zhengyang Zhou, and Yang  
573 Wang. Crossgnn: Confronting noisy multivariate time series via cross interaction refinement.  
574 *Advances in Neural Information Processing Systems*, 36:46885–46902, 2023.
- 575 Jiawei Jiang, Chengkai Han, Wenjun Jiang, Wayne Xin Zhao, and Jingyuan Wang. Libcity: A uni-  
576 fied library towards efficient and comprehensive urban spatial-temporal prediction. *arXiv preprint  
577 arXiv:2304.14343*, 2023.
- 578 Ming Jin, Yu Zheng, Yuan-Fang Li, Siheng Chen, Bin Yang, and Shirui Pan. Multivariate time  
579 series forecasting with dynamic graph neural odes. *IEEE Transactions on Knowledge and Data  
580 Engineering*, 2022.
- 581 Thomas N Kipf and Max Welling. Semi-supervised classification with graph convolutional net-  
582 works. *arXiv preprint arXiv:1609.02907*, 2016.
- 583 Johannes Klicpera, Aleksandar Bojchevski, and Stephan Günnemann. Predict then propagate: Com-  
584 bining neural networks with personalized pagerank for classification on graphs. In *International  
585 conference on learning representations*, 2018.
- 586 Runlin Lei, Zhen Wang, Yaliang Li, Bolin Ding, and Zhewei Wei. Evennet: Ignoring odd-hop neigh-  
587 bors improves robustness of graph neural networks. *Advances in Neural Information Processing  
588 Systems*, 35:4694–4706, 2022.
- 589  
590  
591  
592  
593

- 594 Yaguang Li, Rose Yu, Cyrus Shahabi, and Yan Liu. Diffusion convolutional recurrent neural net-  
595 work: Data-driven traffic forecasting. *arXiv preprint arXiv:1707.01926*, 2017.  
596
- 597 Hangchen Liu, Zheng Dong, Renhe Jiang, Jiewen Deng, Jinliang Deng, Quanjun Chen, and Xuan  
598 Song. Spatio-temporal adaptive embedding makes vanilla transformer sota for traffic forecast-  
599 ing. In *Proceedings of the 32nd ACM international conference on information and knowledge*  
600 *management*, pp. 4125–4129, 2023a.
- 601 Xu Liu, Yuxuan Liang, Chao Huang, Hengchang Hu, Yushi Cao, Bryan Hooi, and Roger Zim-  
602 mermann. Do we really need graph neural networks for traffic forecasting? *arXiv preprint*  
603 *arXiv:2301.12603*, 2023b.  
604
- 605 Yong Liu, Tengge Hu, Haoran Zhang, Haixu Wu, Shiyu Wang, Lintao Ma, and Mingsheng Long.  
606 itransformer: Inverted transformers are effective for time series forecasting. *arXiv preprint*  
607 *arXiv:2310.06625*, 2023c.
- 608 Yuqi Nie, Nam H Nguyen, Phanwadee Sinthong, and Jayant Kalagnanam. A time series is worth 64  
609 words: Long-term forecasting with transformers. *arXiv preprint arXiv:2211.14730*, 2022.  
610
- 611 Xihao Piao, Zheng Chen, Taichi Murayama, Yasuko Matsubara, and Yasushi Sakurai. Fredformer:  
612 Frequency debiased transformer for time series forecasting. In *Proceedings of the 30th ACM*  
613 *SIGKDD Conference on Knowledge Discovery and Data Mining*, pp. 2400–2410, 2024.
- 614 Xiangfei Qiu, Jilin Hu, Lekui Zhou, Xingjian Wu, Junyang Du, Buang Zhang, Chenjuan Guo, Aoy-  
615 ing Zhou, Christian S Jensen, Zhenli Sheng, et al. Tfb: Towards comprehensive and fair bench-  
616 marking of time series forecasting methods. *arXiv preprint arXiv:2403.20150*, 2024.  
617
- 618 Amin Shabani, Amir Abdi, Lili Meng, and Tristan Sylvain. Scaleformer: Iterative multi-scale refin-  
619 ing transformers for time series forecasting. *arXiv preprint arXiv:2206.04038*, 2022.  
620
- 621 Chao Shang, Jie Chen, and Jinbo Bi. Discrete graph structure learning for forecasting multiple time  
622 series. *arXiv preprint arXiv:2101.06861*, 2021.
- 623 Zezhi Shao, Zhao Zhang, Fei Wang, Wei Wei, and Yongjun Xu. Spatial-temporal identity: A simple  
624 yet effective baseline for multivariate time series forecasting. In *Proceedings of the 31st ACM*  
625 *International Conference on Information & Knowledge Management*, pp. 4454–4458, 2022a.  
626
- 627 Zezhi Shao, Zhao Zhang, Wei Wei, Fei Wang, Yongjun Xu, Xin Cao, and Christian S Jensen. De-  
628 coupled dynamic spatial-temporal graph neural network for traffic forecasting. *arXiv preprint*  
629 *arXiv:2206.09112*, 2022b.
- 630 Zezhi Shao, Fei Wang, Yongjun Xu, Wei Wei, Chengqing Yu, Zhao Zhang, Di Yao, Guangyin Jin,  
631 Xin Cao, Gao Cong, et al. Exploring progress in multivariate time series forecasting: Compre-  
632 hensive benchmarking and heterogeneity analysis. *arXiv preprint arXiv:2310.06119*, 2023.  
633
- 634 Daniel Spielman. Spectral and algebraic graph theory. *Yale lecture notes, draft of December*, 4:47,  
635 2019.
- 636 Joel A Tropp. A mathematical introduction to compressive sensing book review. *Bull. Am. Math.*  
637 *Soc*, 54(1):151–165, 2017.  
638
- 639 Yuxuan Wang, Haixu Wu, Jiayang Dong, Yong Liu, Yunzhong Qiu, Haoran Zhang, Jianmin Wang,  
640 and Mingsheng Long. Timexer: Empowering transformers for time series forecasting with ex-  
641 ogenous variables. *arXiv preprint arXiv:2402.19072*, 2024.
- 642 Felix Wu, Amauri Souza, Tianyi Zhang, Christopher Fifty, Tao Yu, and Kilian Weinberger. Sim-  
643 plifying graph convolutional networks. In *International conference on machine learning*, pp.  
644 6861–6871. PMLR, 2019a.  
645
- 646 Haixu Wu, Jiehui Xu, Jianmin Wang, and Mingsheng Long. Autoformer: Decomposition trans-  
647 formers with auto-correlation for long-term series forecasting. *Advances in neural information*  
*processing systems*, 34:22419–22430, 2021.

- 648 Haixu Wu, Tengge Hu, Yong Liu, Hang Zhou, Jianmin Wang, and Mingsheng Long. Timesnet: Tem-  
 649 poral 2d-variation modeling for general time series analysis. *arXiv preprint arXiv:2210.02186*,  
 650 2022.
- 651 Zonghan Wu, Shirui Pan, Guodong Long, Jing Jiang, and Chengqi Zhang. Graph wavenet for deep  
 652 spatial-temporal graph modeling. *arXiv preprint arXiv:1906.00121*, 2019b.
- 653 Zonghan Wu, Shirui Pan, Guodong Long, Jing Jiang, Xiaojun Chang, and Chengqi Zhang. Con-  
 654 necting the dots: Multivariate time series forecasting with graph neural networks. In *Proceedings*  
 655 *of the 26th ACM SIGKDD international conference on knowledge discovery & data mining*, pp.  
 656 753–763, 2020.
- 657 Chin-Chia Michael Yeh, Yujie Fan, Xin Dai, Uday Singh Saini, Vivian Lai, Prince Osei Aboagye,  
 658 Junpeng Wang, Huiyuan Chen, Yan Zheng, Zhongfang Zhuang, et al. Rpmixer: Shaking up time  
 659 series forecasting with random projections for large spatial-temporal data. In *Proceedings of the*  
 660 *30th ACM SIGKDD Conference on Knowledge Discovery and Data Mining*, 2024.
- 661 Bing Yu, Haoteng Yin, and Zhanxing Zhu. Spatio-temporal graph convolutional networks: A deep  
 662 learning framework for traffic forecasting. *arXiv preprint arXiv:1709.04875*, 2017.
- 663 Ailing Zeng, Muxi Chen, Lei Zhang, and Qiang Xu. Are transformers effective for time series  
 664 forecasting? *arXiv preprint arXiv:2205.13504*, 2022.
- 665 Yunhao Zhang and Junchi Yan. Crossformer: Transformer utilizing cross-dimension dependency  
 666 for multivariate time series forecasting. In *The eleventh international conference on learning*  
 667 *representations*, 2023.
- 668 Yanping Zheng, Lu Yi, and Zhewei Wei. A survey of dynamic graph neural networks. *arXiv preprint*  
 669 *arXiv:2404.18211*, 2024.
- 670 Haoyi Zhou, Shanghang Zhang, Jieqi Peng, Shuai Zhang, Jianxin Li, Hui Xiong, and Wancai Zhang.  
 671 Informer: Beyond efficient transformer for long sequence time-series forecasting. In *Proceedings*  
 672 *of the AAAI conference on artificial intelligence*, volume 35, pp. 11106–11115, 2021.

## 678 A APPENDIX



689 Figure 9: Visualization of learned graph filters. The results show that the filters of the adaptive graph  
 690 resemble a band-rejection filter across public datasets, indicating the presence of both homophilic  
 691 and heterophilic relationships between nodes.

692  
 693  
 694  
 695  
 696  
 697  
 698  
 699  
 700  
 701

Table 3: Comparison of existing models on short-term STF and long-term STF results. Existing models struggle to balance prediction accuracy and training efficiency when handling long-term STF tasks. FLOPs:  $\times 10^3$ .

Methods		Ours		STID		D2STGNN		STAEformer		MTGNN		StemGNN	
Metric		12-12	96-12	12-12	96-12	12-12	96-12	12-12	96-12	12-12	96-12	12-12	96-12
PEMS03	MAE	<b>14.42</b>	<b>14.32</b>	15.51	15.10	<u>14.80</u>	NA	14.86	NA	14.85	14.64	16.51	57.83
	RMSE	<b>24.92</b>	<u>24.29</u>	27.33	26.56	25.82	NA	25.57	NA	25.23	<b>23.91</b>	27.72	83.53
	MAPE	<u>14.89%</u>	<u>15.29%</u>	16.02%	16.51%	15.15%	NA	15.02%	NA	<b>14.55%</b>	<b>15.20%</b>	16.92%	176.31%
	FLOPs	4.79	4.82	1.14	1.22	141	NA	184.30	NA	4.86	52.75	12.39	759.50
PEMS04	MAE	<b>18.05</b>	<b>18.16</b>	18.22	<u>18.31</u>	18.31	NA	<u>18.18</u>	NA	19.13	18.79	24.02	72.65
	RMSE	30.60	<b>29.74</b>	<u>30.33</u>	<u>29.76</u>	<b>29.82</b>	NA	30.24	NA	31.03	30.55	37.04	104.81
	MAPE	<b>11.92%</b>	<b>12.51%</b>	<u>11.99%</u>	<u>12.53%</u>	12.29%	NA	12.29%	NA	13.22%	13.02%	17.63%	54.88%
	FLOPs	2.66	2.67	0.64	0.68	69.04	NA	99.30	832.70	2.71	29.36	6.86	422.40
PEMS07	MAE	<b>19.03</b>	<b>19.10</b>	19.31	<u>19.44</u>	19.55	NA	<u>19.22</u>	NA	21.01	20.81	22.72	75.73
	RMSE	<b>32.34</b>	<b>32.21</b>	32.95	<u>32.46</u>	32.83	NA	<u>32.54</u>	NA	34.14	33.83	36.99	106.81
	MAPE	<b>8.00%</b>	<b>8.08%</b>	8.05%	<u>8.28%</u>	8.23%	NA	<u>8.03%</u>	NA	8.92%	9.05%	9.57%	82.70%
	FLOPs	13.33	13.41	3.03	3.25	884.00	NA	660.60	NA	12.90	140.00	35.69	2032.00
PEMS08	MAE	<u>13.72</u>	<b>13.70</b>	14.12	<u>14.11</u>	14.20	NA	<b>13.60</b>	NA	15.25	14.93	16.37	69.20
	RMSE	<b>23.30</b>	<b>22.88</b>	23.88	<u>23.27</u>	<u>23.65</u>	NA	23.45	NA	24.22	23.89	26.13	92.56
	MAPE	<u>8.98%</u>	<b>9.10%</b>	9.21%	<u>9.30%</u>	9.26%	NA	<b>8.94%</b>	NA	10.66%	10.21%	10.71%	104.44%
	FLOPs	1.54	1.55	0.37	0.40	25.83	442.40	52.25	440.90	1.57	17.02	3.93	245.30
SD	MAE	<b>17.53</b>	<b>15.58</b>	17.86	<u>16.74</u>	17.72	NA	18.96	NA	18.61	17.11	23.52	74.25
	RMSE	<u>31.29</u>	<b>26.85</b>	31.42	<u>29.07</u>	<b>29.91</b>	NA	34.89	NA	31.57	29.50	38.05	108.82
	MAPE	<b>11.31%</b>	<b>10.11%</b>	11.84%	<u>11.36%</u>	11.89%	NA	12.26%	NA	12.81%	11.84%	15.98%	74.55%
	FLOPs	13.16	13.25	3.05	3.28	717.40	NA	610.20	NA	12.99	141.20	34.92	2043.00

756  
 757  
 758  
 759  
 760  
 761  
 762  
 763  
 764  
 765  
 766  
 767  
 768  
 769  
 770  
 771  
 772  
 773  
 774  
 775  
 776  
 777  
 778  
 779  
 780  
 781  
 782  
 783  
 784  
 785  
 786  
 787  
 788  
 789  
 790  
 791  
 792  
 793  
 794  
 795  
 796  
 797  
 798  
 799  
 800  
 801  
 802  
 803  
 804  
 805  
 806  
 807  
 808  
 809

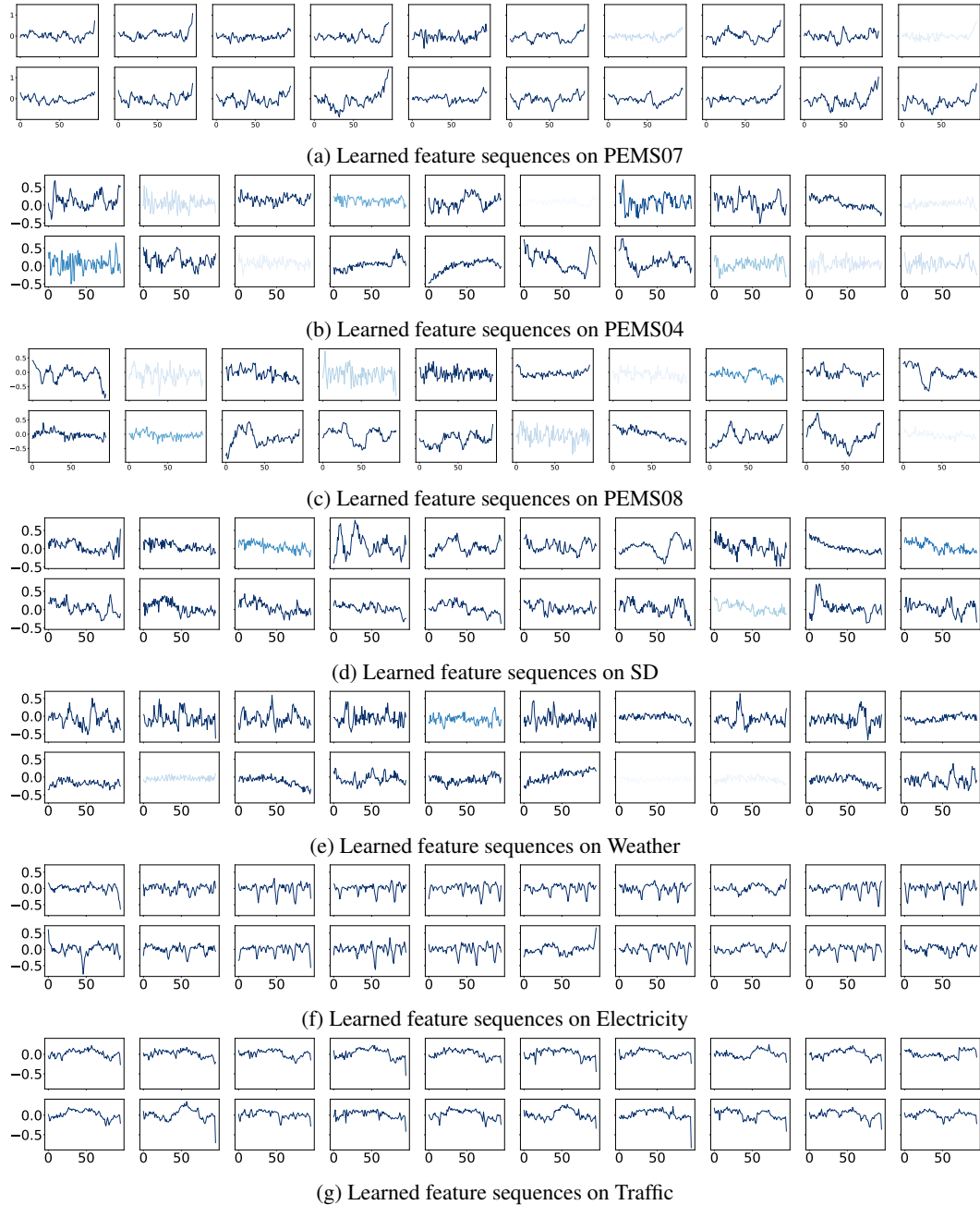
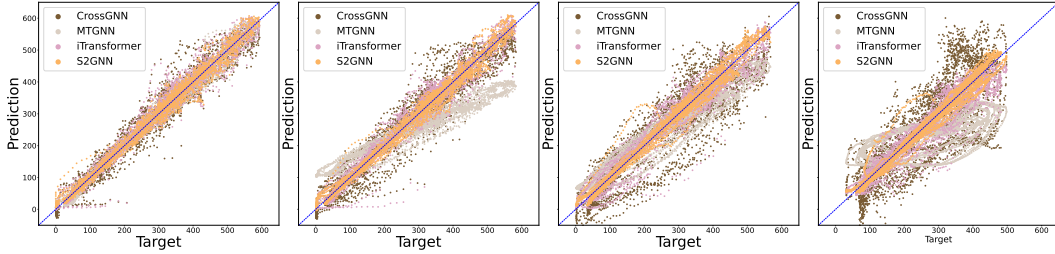
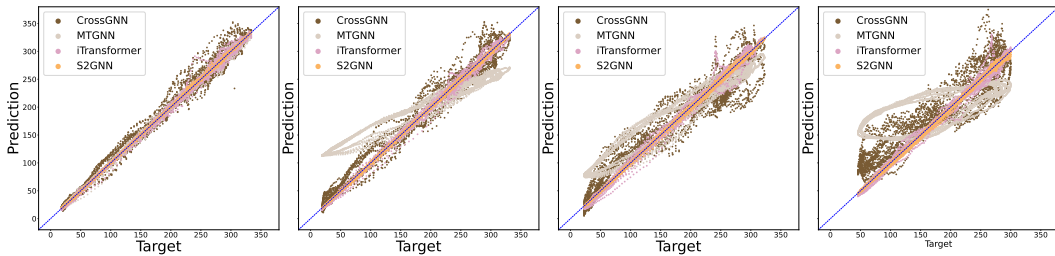


Figure 10: More visualizations of the convolutional kernels used in the cross-correlation embedding process, where the color intensity represents their usage frequency (i.e., the number of times each kernel is connected).

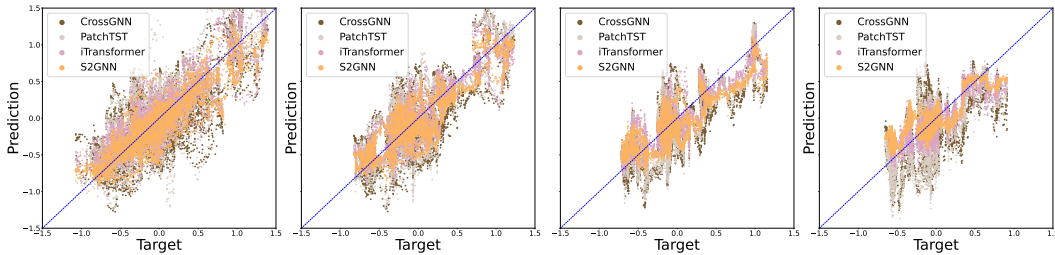
810  
811  
812  
813  
814  
815  
816  
817  
818  
819  
820  
821  
822  
823  
824  
825  
826  
827  
828  
829  
830  
831  
832  
833  
834  
835  
836  
837  
838  
839  
840  
841  
842  
843  
844  
845  
846  
847  
848  
849  
850  
851  
852  
853  
854  
855  
856  
857  
858  
859  
860  
861  
862  
863



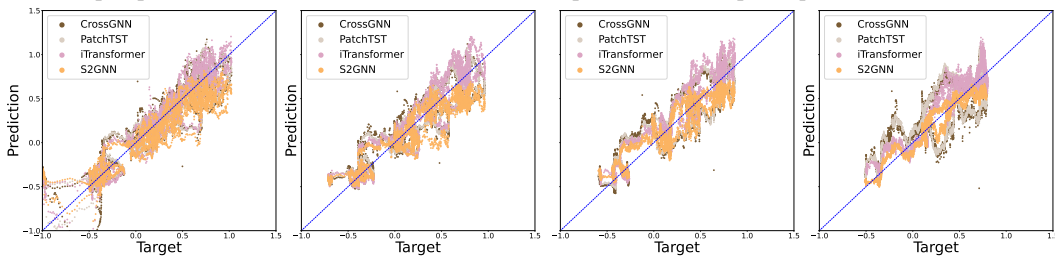
(a) More Examples of PEMS04 dataset. We use the 201st node for the sake of simplicity. From left to right, the results depict predictions for 12, 24, 48, and 96 time steps based on an input sequence of 96.



(b) More Examples of PEMS04 dataset. We use the 150th node for the sake of simplicity. From left to right, the results depict predictions for 12, 24, 48, and 96 time steps based on an input sequence of 96.



(c) More examples of Electricity dataset. We use the 50th node for the sake of simplicity. From left to right, the results depict predictions for 96, 192, 336, and 720 time steps based on an input sequence of 96.



(d) More examples of Electricity dataset. We use the 150th node for the sake of simplicity. From left to right, the results depict predictions for 96, 192, 336, and 720 time steps based on an input sequence of 96.

Figure 11: More comparison between the prediction results and the target values. Each data point represents the average of the predicted results and the true values over the given sequence.